# Time-Resolved Digital Immunoassay for Rapid and Sensitive Quantitation of Procalcitonin with Plasmonic Imaging

*Wenwen Jing[1]†, Yan Wang[1]†, Yunze Yang[1], Yi Wang[2], Guangzhong Ma[1], Shaopeng Wang[1] and Nongjian Tao [*1,3]*

[1]Biodesign Center for Biosensors and Bioelectronics, Arizona State University, Tempe, Arizona 85287, USA.

[2]State Key Laboratory of Analytical Chemistry for Life Science, School of Chemistry and Chemical Engineering, Nanjing University, Nanjing 210093, China.

[3]School of Electrical, Computer and Energy Engineering, Arizona State University, Tempe, Arizona 85287, USA.

† W.J. and Y.W. contributed equally to this work.

## Supporting Information

**S1. Protocol of TD-immunoassay.** Figure S1 shows the protocol of the immunoassay reaction used in the present work for PCT detection. The capture antibody was pre-coated on a sensor surface (gold –coated glass slide) using the steps shown in Fig. S1a, which is similar to that for commercial SPR sensor chips. The capture antibody-coated sensor was exposed to 100 µL standard or sample and incubated for 10 min, followed by washing with PBST buffer (Fig. S1b). 100 µL biotinylated PCT detection antibody was then added and incubated for 10 min. After washing 100 µL streptavidin-coated GNP solution ($9.41\times10^8$ GNPs per well) was added (~530 streptavidin molecules are covalently coated on each GNP), during which plasmonic imaging was performed for 5 min.

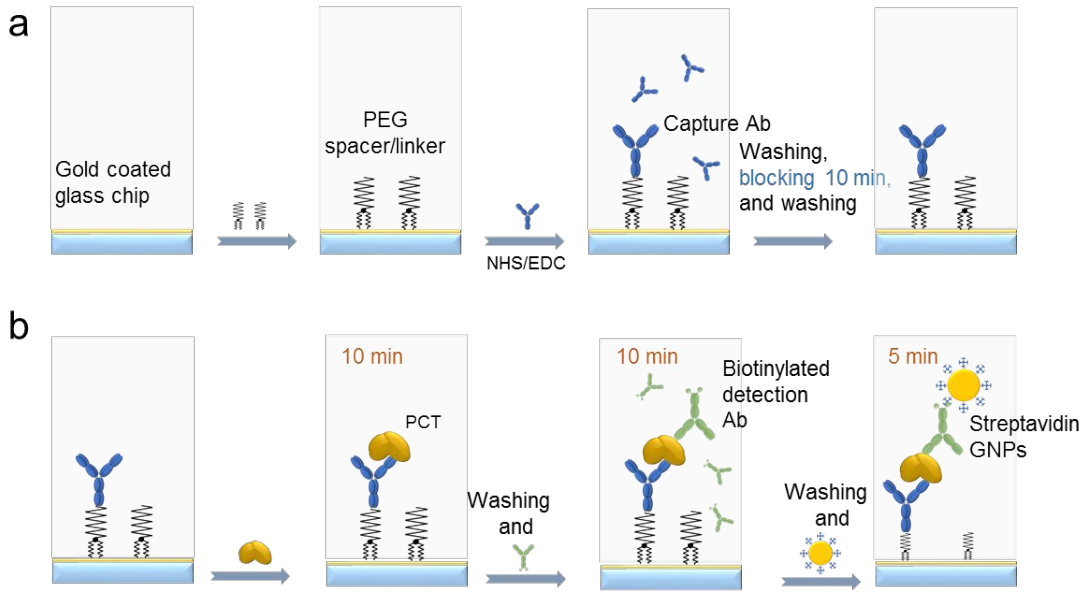


**Figure S1. Protocol of TD-immunoassay. (a)** Preparation of capture-antibody coated sensor surface for PCT detection. **(b)** Steps for the PCT assay with TD-immunoassay.

**S2. Time-resolved tracking of single nanoparticles with plasmonic imaging.** Manual counting of each nanoparticle bound on the gold surface over time is impossible because each test includes 30,000 to 130,000 frames of plasmonic images, and each frame contains a large number of nanoparticles with both binding and unbinding events taking place at the same time. An imaging-processing algorithm was developed to automatically count the binding and unbinding events using the steps shown in Fig. S2. Step 1:

Background noise was removed by first applying the K-space filtering process (due to special pattern of GNP plasmonic image[1]), then averaging consecutive blocks and subtracting the previous from the current one to generate differential image sequences. Shot noise was reduced by maximizing the number of photons in the differential images.[2,3] Step 2: To automatically identify and count each nanoparticle in an image, a template was chosen from a pre-processed image sequence and used to correlate with each frame. To eliminate the influence of light intensity, template matching was achieved by normalizing the template and the images to be processed.[4] The binding and unbinding of nanoparticles on each image frame were determined by finding a local maximum in the correlation image. To avoid drift of the images, the algorithm automatically updated the template after a certain period of time. Occasionally, the plasmonic image of a nanoparticle was detected as fluctuating (binding and unbinding). These rare events (<0.1%) were detected but removed from counting. Step 3: From the template-matched patterns on each image frame, nanoparticles associated with binding and unbinding determined, from which the net number of nanoparticles bound to the surface was counted.

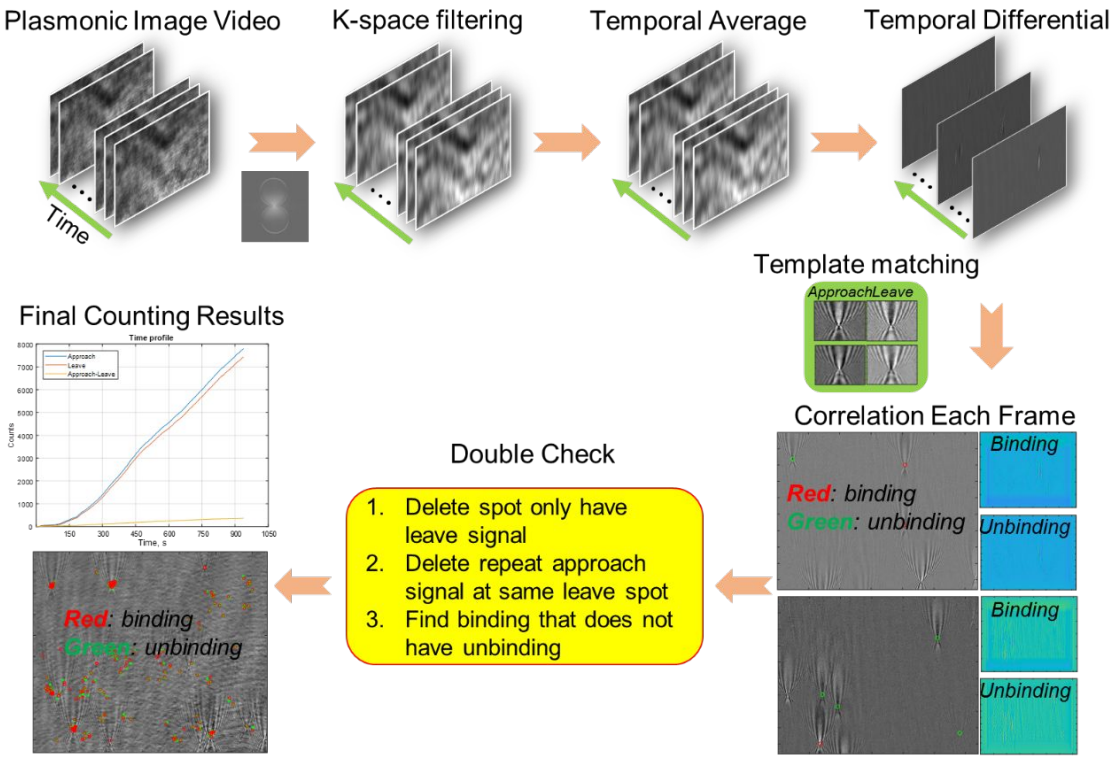


**Figure S2. Automatic particle counting algorithm.** Step 1: Pre-processing plasmonic images using K-space filtering, temporal subtraction and shot noise reduction. Step 2: Identifying nanoparticle with a template-matching algorithm. Step 3: Detect binding and unbinding events. See text for more details.

**S3. TD-immunoassay detection of IgG/anti-IgG binding.** The standard curve of the IgG/anti-IgG binding can be fitted with an empirical equation widely used in ELISA, which is given by

$$y = A_2 + \frac{A_1 - A_2}{1 + (\frac{X}{X_0})^p} \qquad (2)$$

with r-square of 0.9986 (Fig. 2e).

**S4. Evaluation of time dependence of TD-immunoassay**

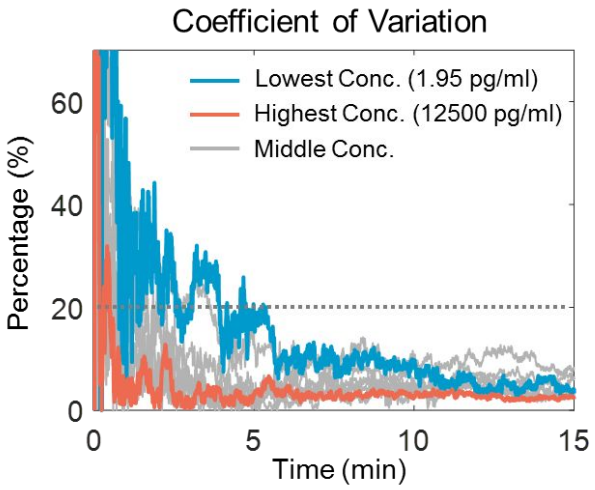


**Figure S3. Evaluation of time dependence of TD-immunoassay.** Time dependence of coefficient of variation for PCT time in the present TD-immunoassay measurements, where the dotted horizontal line indicates 20% coefficient of variation.

S5. Standard curve of conventional ELISA for PCT detection

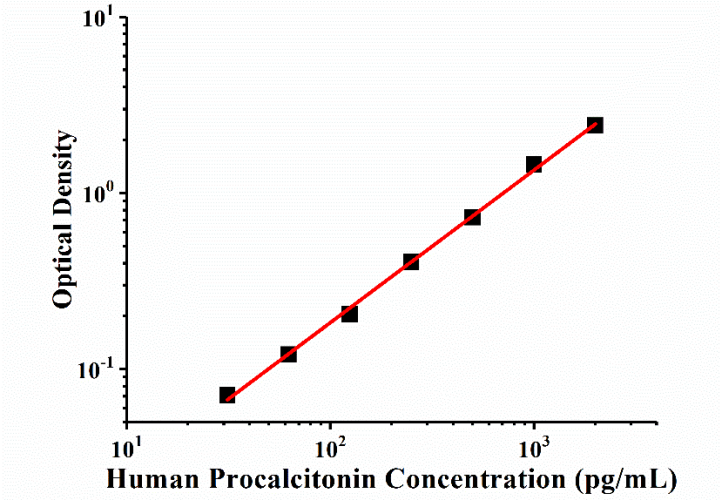


**Figure S4. Standard curve of PCT detection measured by conventional ELISA**. Log-log plot of signal output (r-square = 0.9986 showing a response of 2 logs, range from 31.3 pg/mL to 2000 pg/mL following the instructions of the ELISA kit.

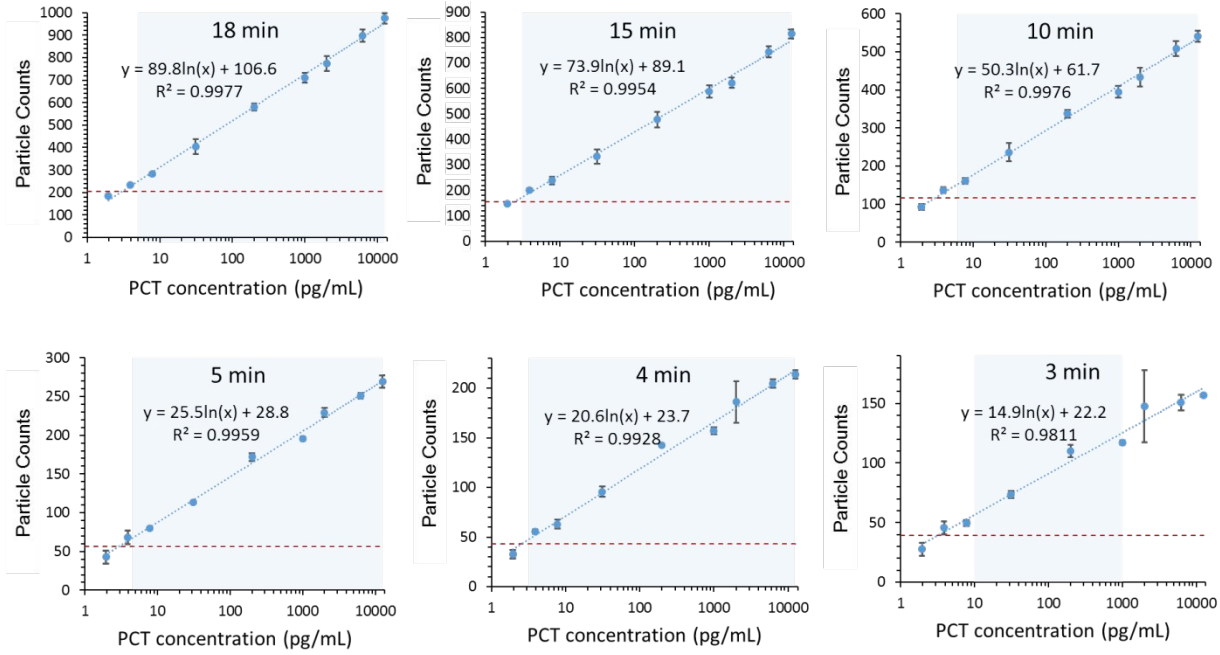


**Figure S5. Standard curve of PCT detection at different time points,** where the horizontal dashed lines show the limit of detection, shaded areas represent the dynamic range, and the error bars are the standard deviation over triplicate test. Because the PCT levels of sepsis patients are usually lower than 10000 pg/mL, PCT concentrations higher than 12500 pg/mL were not tested.

## S6. Dynamic range of TD-immunoassay

TD-immunoassay features differential imaging with real-time information, and it quantifies the GNP number change per unit time. The actual dynamic range of TD-immunoassay can be several orders greater than what was demonstrated in the present work. For an imaging frame rate of 26.6 fps, the temporal resolution is 37.6 ms, within which up to $5\times10^3$ GNPs per field of view (~ $4.6 \times 10^3$ $\mu m^2$) can be resolved if assuming optical diffraction limit ~278 nm for each particle spot. This corresponds to ~$10^5$ GNPs/sec as the upper limit. The lower limit is the detection of a single GNP. For time interval of 10 min, the lower limit (a single GNP detected in the 10 minutes period) in the detection of GNP binding rate is $1.67x10^{-3}$ GNP/sec. The full dynamic range of detection is thus about $6\times10^7$. This wide dynamic range covers the requirement of most immunoassay applications. The above discussion assumes 10 min time interval for GNP counting, which can be tuned based on the need of detection time and dynamic range. Because TD-immunoassay also involves incubation of biomarkers with capture antibody, which can also be adjusted based on the need of detection limit, detection time and dynamic range.

## S7. Statistical Analysis

We used the linear regression model for PCT counting error prediction, given by

$$N = \beta_0 + \beta_1 \log(c) + \epsilon, \qquad (1)$$

where $N$ is particle counts, $c$ is the PCT concentration, $\beta_0$ and $\beta_1$ are constants and $\epsilon$ describes the error. Given the measurement error $\epsilon$ is mostly affected by the counting error, which depends on particle counts $N$, given by $\epsilon \sim N(0, \sigma^2 Y)$, we transform the heteroscedastic model into a homoscedastic model for the linear regression analysis:

$$\sqrt{N} = \sqrt{\beta_0 + \beta_1 \log(c)} + \epsilon_0, \ \epsilon_0 \sim N(0, \sigma^2), \quad (2)$$

We use 95% prediction interval to evaluate the prediction accuracy from the counting numbers.

## S8. Surface densities of capture antibody, PCT and detection antibody, and molecular spacing of PCT on the sensor surface

We determined the surface densities of the capture antibody, PCT molecules and detection antibody using conventional SPR. We calibrated the plasmonic response by changing the buffer from 1× PBS to 0.9× PBS buffer, and found that 1 mDeg resonant angle shift corresponded to a mass density change of 10 pg/mm$^2$. This allowed us to determine the coverage of the capture antibody to be 332.4 pg/mm$^2$ from the SPR response [5-7] (Figure S6a). Similarly, the mass densities for PCT with an initial solution concentration of 1.25 × 10$^4$ pg/mL and detection antibody with an initial solution concentration of 50 ng/mL in 10 min are 9 pg/mm$^2$ and ~12 pg/mm$^2$, respectively (Figures S6b and c). From the molecular weights of the capture antibody (150 kDa), PCT (14.5 kDa), and detection antibody (150 kDa), we converted the mass densities to number densities, and then determined the average molecular spacing for each case (Table S1).

1.25x10$^4$ pg/mL was the maximum PCT concentration measured in the experiment, and the corresponding molecular spacings for PCT and detection antibody are thus the lower limits. For the detection antibody, the lower limit of the molecular spacing is 146 nm. For a GNP to simultaneously bind to two PCT molecules, the average

distance between two detection antibody molecules must be smaller than $2\sqrt{2Rd-d^2}$, which is ~108 nm for 150 nm-diameter GNPs (Figure S7). Base on this estimation, the likelihood of one GNP to bind to two PCT molecules is low, especially for PCT concentrations <1.25x10$^4$ pg/mL.

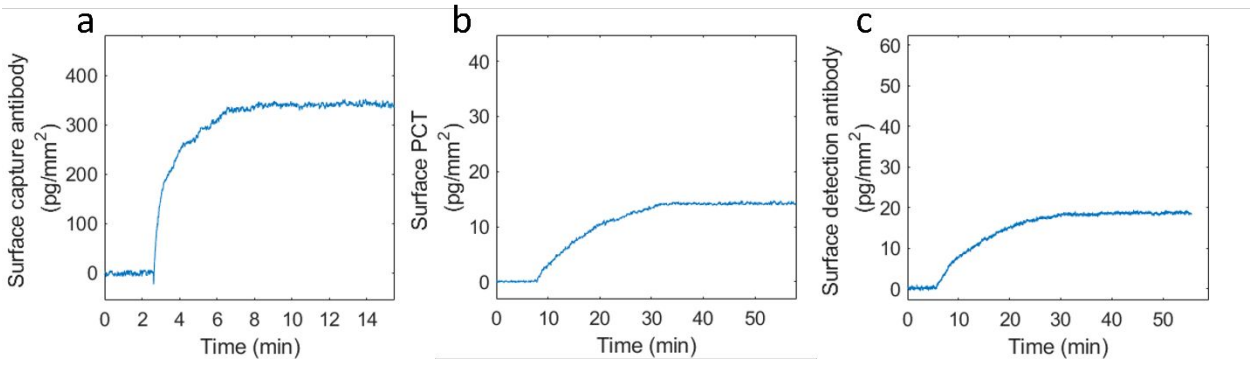


**Figure S6. SPR data showing mass density changes of capture antibody (a), PCT (b), and detection antibody (c) in 10 min. These data were measured on a commercial instrument (Biosensing Instrument. Model: SPRM 200 SERIES).**

**Table S1. Determination of molecular spacings of capture antibody, PCT and detection antibody.**

| | Surface density (molecules/$\mu m^2$) | Coverage area per molecule ($nm^2$/molecule) | Molecular spacing (nm) |
|---|---|---|---|
| Capture antibody | 1330 | 752 | ~27 |
| PCT | 373 | 2681 | >52 |
| Detection antibody | 47 | 21277 | >146 |

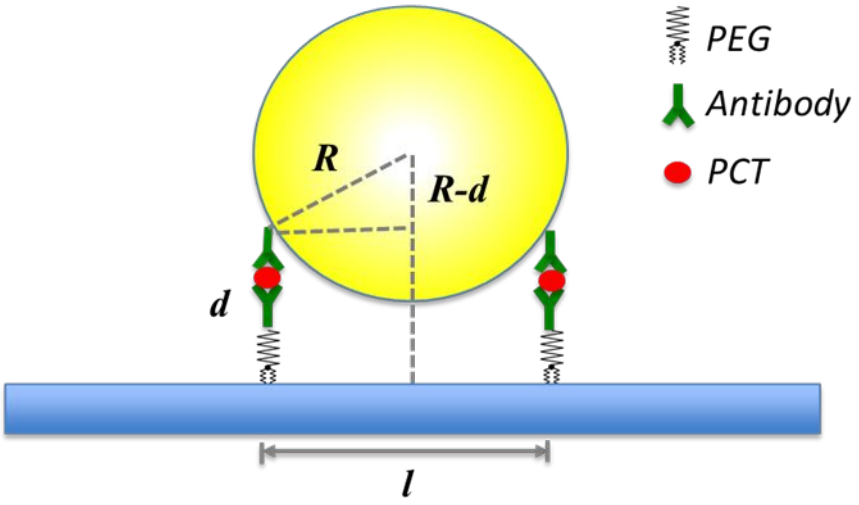


**Figure S7 Geometric consideration of one gold nanoparticle (GNP) binding to two PCT molecules**. The distance (d) between the GNP surface and sensor surface must fit the size of the capture antibody, PCT, detection antibody and PEG used in the conjugation, which are 9 nm, 3 nm, 9 nm and 2 nm, respectively. This leads to d=23 nm. To accommodate binding of two PCT molecules, the PCT molecular spacing must be $l = 2 \times \sqrt{R^2 - (R-d)^2} = 108$ nm.

## S9. Comparison of two different sizes of GNPs

We compared results using GNPs with diameters of 150 nm and 40 nm in sera. The plasmonic image contrast for the 150 nm GNPs is better than the 40 nm GNPs (Figure S8), which was the reason that this work focused on the 150 nm GNPs. However, the particle counts (measure the binding and unbinding events) obtained in 5 mins for the two sizes in a blank solution and in 20 pg/mL are similar.

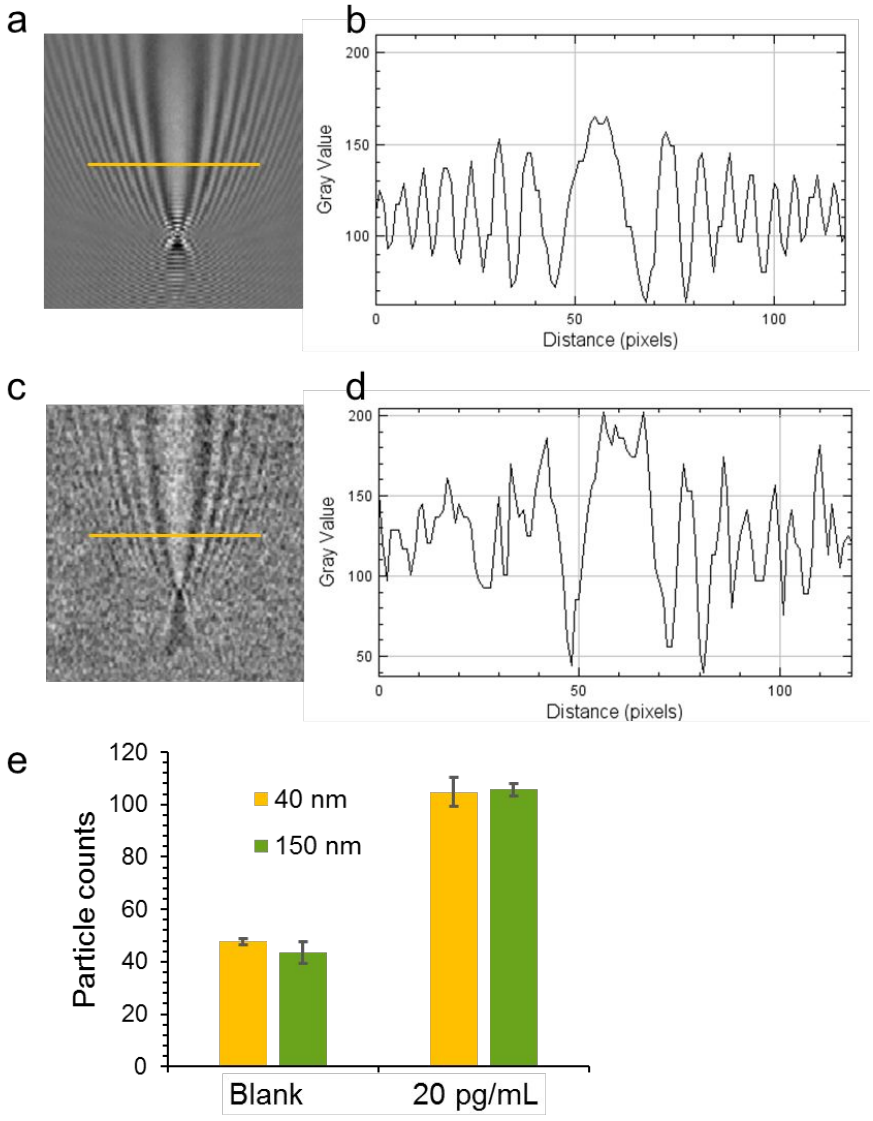


**Figure S8. Comparison of GNPs with diameters of 150 nm and 40 nm in sera.** The plasmonic image contrast for the 150 nm GNPs (a) is better than that of the 40 nm GNPs (c), where the intensity profiles along the lines in a and b are plotted in b and c. The particle counts for the 150 nm and 40 nm GNPs obtained in 5 min in a blank solution, and in 20 pg/mL PCT spiked in sera are similar (e).

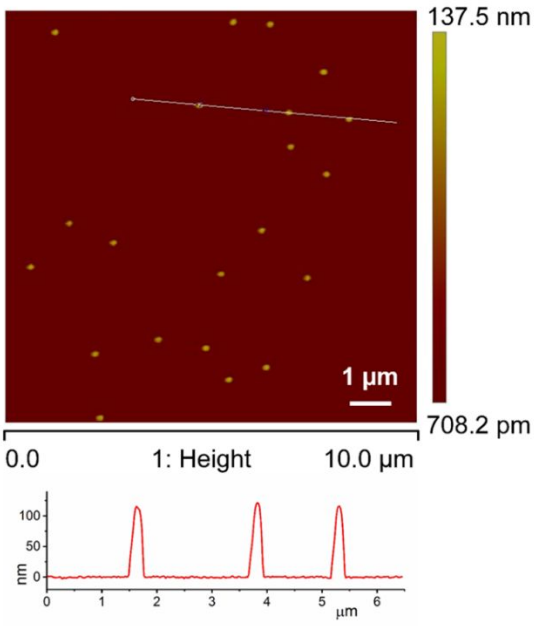


**Figure S9.** AFM image of the gold nanoparticles onto the surface. The AFM image shows that all the gold nanoparticles are single and uniformly distributed on the surface. This is well proved that each SPR signal is generated from one gold nanoparticle rather than conjugated gold nanoparticles.

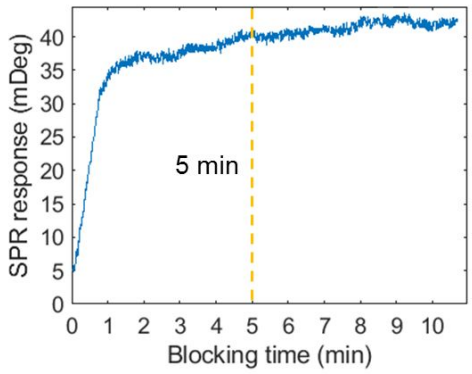


**Figure S10. Monitoring of blocking (1% BSA) with SPR, showing that** 5 min is sufficient for effective blocking.

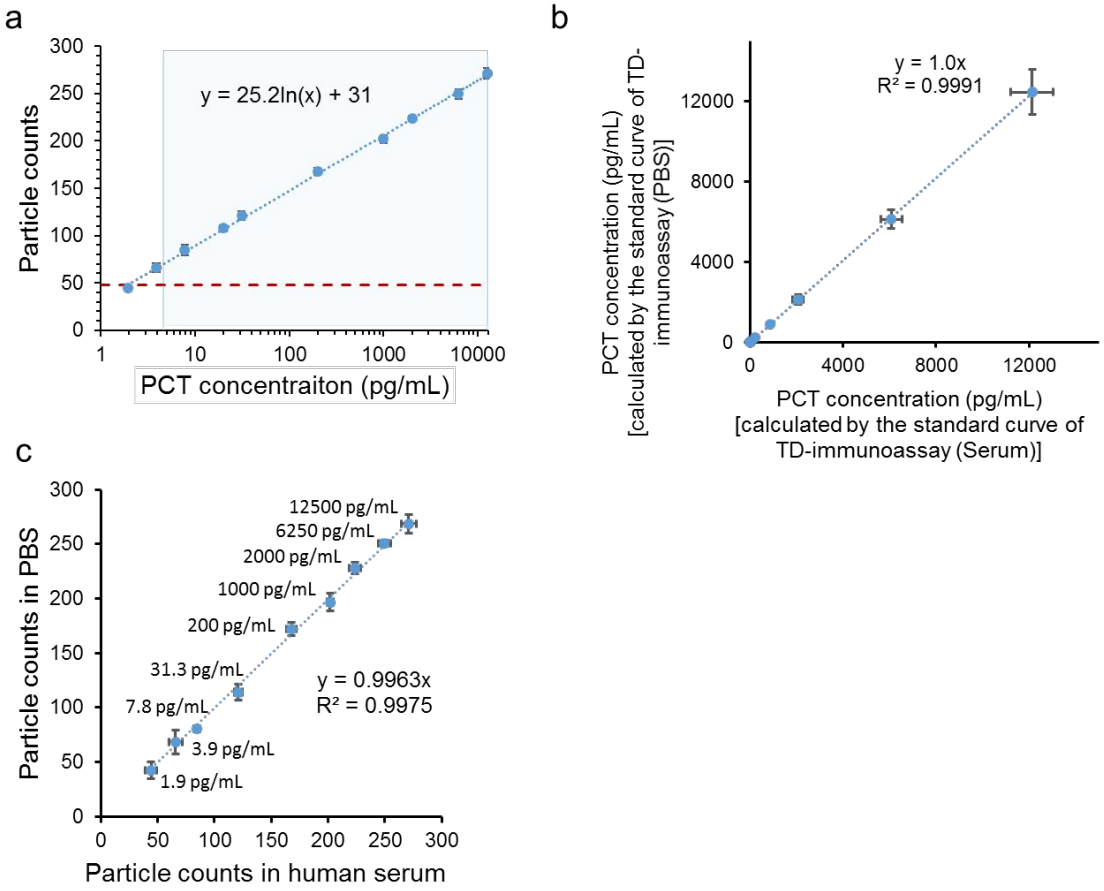

**Figure S11. PCT detection in serum.** (a) Standard curve of PCT detection in sera, where the error bars are the standard deviations from triplicate tests, the dashed lines are fits to the equation shown in the figure, and the shaded area marks the dynamic range. The limit of detection determined by the mean concentration measured for the blank solution plus three times of standard deviation is 2.1 pg/mL (red dashed line in a). The limit of quantification defined by the mean concentration measured for the blank solutions plus ten times of the standard deviation is 4.4 pg/mL. (b) Correlation of PCT spiked human serum using different standard curves, indicating that the concentration of PCT spiked in serum can be measured by the PCT TD-immunoassay standard curve. (c) Correlation of PCT spiked human serum with PCT spiked PBS showing similar results for PCT spiked in serum and in PBS. In our present case, the incubation time short, compared to traditional ELISA, which helps reduce non-specific binding. This is a likely reason for the observed similar detection limit. However, this may not be a general conclusion because non-specific binding depends on the surface chemistry of the chip, quality of the antibody and gold nanoparticle.

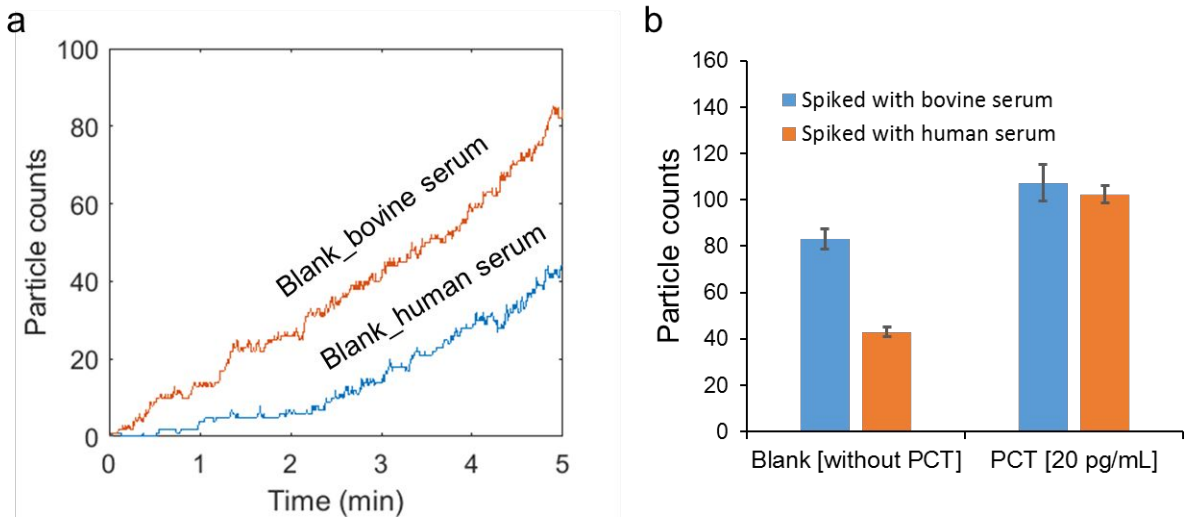


**Figure S12. Comparison between PCT-spiked human serum and PCT-spiked bovine serum (non-human PCT).** (a) Particle counts of blank bovine and blank human sera vs. time (no PCT added serum). (b) Particle counts for blank and 20 pg/mL PCT spiked bovine and human sera. The non-specific binding of bovine sera is higher than that of the human sera. This is likely due to that the antibody kits we used were specific for human IgG only. However, we have carried out additional tests in PBS and human sera (Figure S11), and found that at zero PCT concentration, the results of the both samples are similar, indicating the level of PCT in the sera is low.

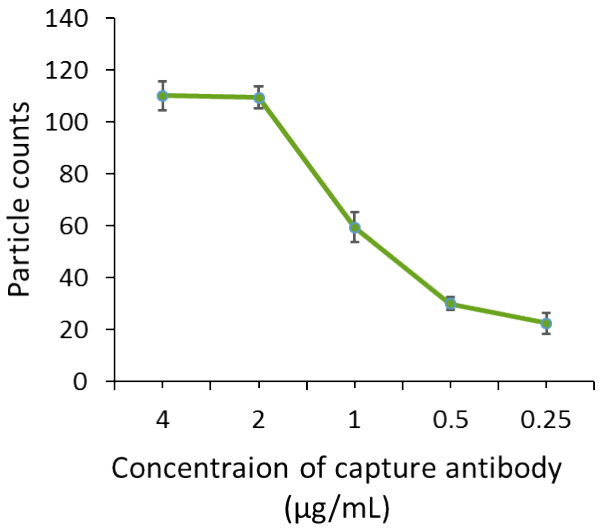


**Figure S13. Dependence of particle counts on capture antibody concentration in 10 min.**

For capture antibody with concentrations of 2 μg/mL or higher, the particle counts are similar. For this reason, we selected 2 μg/mL capture antibody for PCT detection.

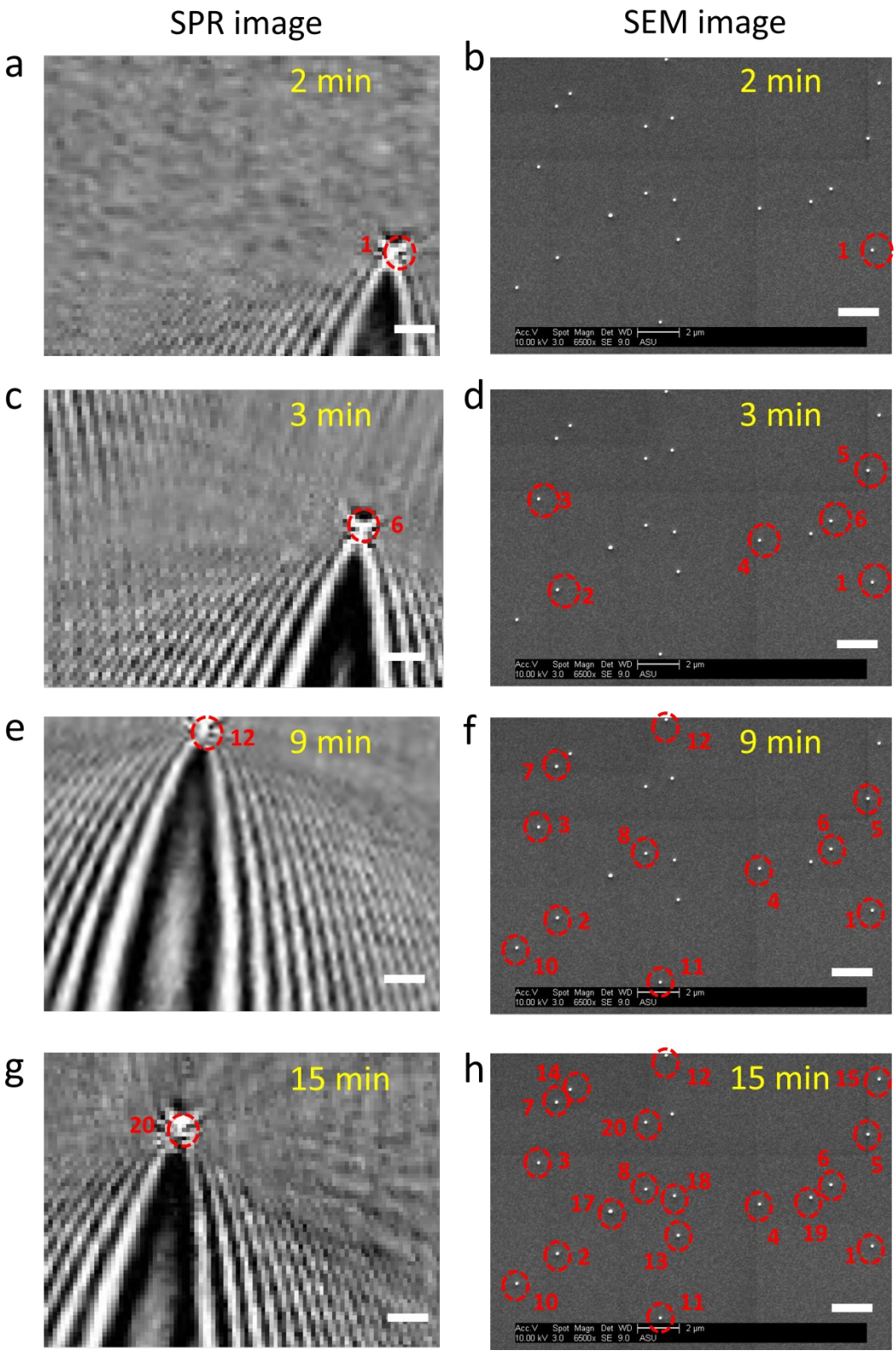
SPR image
SEM image
a
2 min
b
2 min
c
3 min
d
3 min
e
9 min
f
9 min
g
15 min
h
15 min

**Figure S14. Confirmation of SPR binding events with SEM. a, c, e, g** The SPR time differential images show the binding events at 2, 3, 9 and 15 minutes. Only the binding event occurring at this time point can be seen on the SPR time difference image. The red circle is the location of the gold nanoparticles. The numbers next to the circle are the order in which they are bond to the surface (here we randomly select a few of the binding events from all, *i.e.* No. 1, 6, 13 and 20. The rest of the binding events can be found in the support information video S1). **b, d, f, h** The SEM images show the individual gold nanoparticles that left on the gold chip after the binding experiment. All gold nanoparticles that had been bonded to the surface at this time point were marked with red circles and numbers on the SEM images. The scale bar on both SPR image and SEM image is 2 μm. The SPR images and the SEM images show a good correlation for each binding event.

**Video S1. Video after processing.** After image processing, the binding signals be seen from the video which captures the dynamic binding processes of the individual particles. Each particle binding is circled in red, and numbered to mark its position, which matches that on the SEM image. The numbers are the order in which they bind to the surface.

**S10. PCT level of blank human serum.** Low levels of PCT in healthy human sera have been reported[8]. To verify the presence of PCT in the blank human serum used in this study, we tested the healthy human serum with an ELISA kit (Abcam. ab221828 Human Procalcitonin SimpleStep ELISA® Kit). Figure S15 shows the standard curve obtained from this kit measured by the conventional ELISA method ($R^2$ of the fitting is 0.99). From the standard curve, we determined the PCT level in the healthy human serum, which is minimal as shown in Table S2.

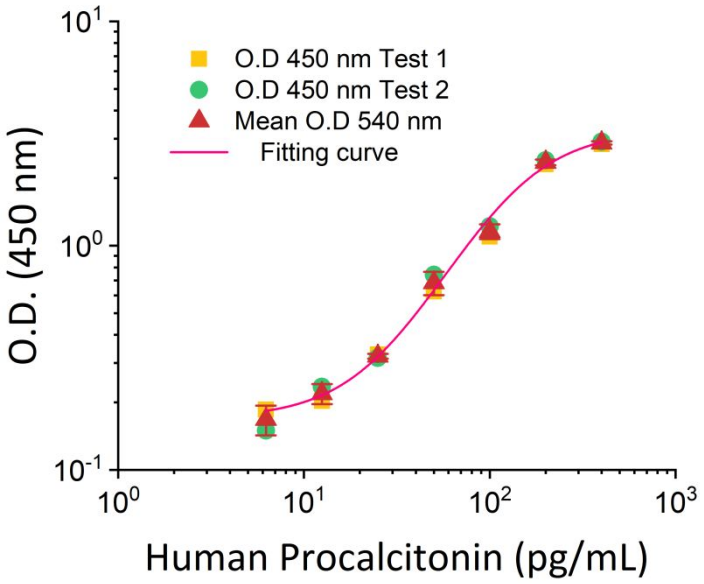

Figure S15. PCT standard curve obtained from conventional ELISA using a highly sensitive ELISA kit.

Table S2. PCT level of blank human serum.

| O.D 450 nm | PCT Concentration (pg/mL) |
|---|---|
| 0.12 | NA |
| 0.194 | 8.7 |
| 0.159 | NA |
| 0.121 | NA |
| 0.179 | NA |
| 0.2 | 9.8 |
| 0.203 | 10.4 |
| 0.095 | NA |
| 0.078 | NA |
| 0.201 | 10 |
| 0.187 | 7.1 |
| 0.138 | NA |
| 0.186 | 6.9 |
| 0.091 | NA |

| | |
|---|---|
| 0.115 | NA |
| 0.095 | NA |
| **Mean O. D 450 nm** | |
| 0.147 | NA |

## REFERENCES


(1) Yu, H.; Shan, X.; Wang, S.; Chen, H.; Tao, N. Molecular Scale Origin of Surface Plasmon Resonance Biosensors. *Anal. Chem.* **2014**, *8992-8997*.

(2) Ortega Arroyo, J.; Cole, D.; Kukura, P. Interferometric Scattering Microscopy and Its Combination with Single-Molecule Fluorescence Imaging. *Nat. Protoc.* **2016**, 617-633.

(3) Young, G.; Hundt, N.; Cole, D.; Fineberg, A.; Andrecka, J.; Tyler, A.; Olerinyova, A.; Ansari, A.; Marklund, E. G.; Collier, M. P.; Chandler S. A.; Tkachenko, O.; Allen, J.; Crispin, M.; Billington, N.; Takagi, Y.; Seller, J. R.; Eichmann, C.; Selenko, P.; Frey, L. *et al.* Quantitative Mass Imaging of Single Biological Macromolecules. *Science* (80-. ). **2018**, *423-+*.

(4) Normalized 2-D cross-correlation-MATLAB normxcorr2. https://www.mathworks.com/help/images/ref/normxcorr2.html. (accessed Octomber 10, 2018).

(5) Tudos, A. J.; Schasfoort, R. B. M. Chapter 1. Introduction to Surface Plasmon Resonance. *Handb. Surf. Plasmon Reson.* **2010**.

(6) Myszka, D. G.; Jonsen, M. D.; Graves, B. J. Equilibrium Analysis of High Affinity Interactions Using BIACORE. *Anal. Biochem.* **1998**, 326-330.

(7) Landry, J. P.; Fei, Y.; Zhu, X. Simultaneous Measurement of 10,000 Protein-Ligand Affinity Constants Using Microarray-Based Kinetic Constant Assays. *Assay Drug Dev. Technol.* **2011**, 250-259.

(8) Shaikh, M. M.; Lucas, E. H.; Jacob, M. V. "Is serum procalcitonin measurement a useful addition to a rheumatologist's repertoire? A review of its diagnostic role in systemic inflammatory diseases and joint infections." *Rheumatology.* **2014**, 231-240.